Journal of Applied Fluid Mechanics, Vol. 15, No. 3, pp. 645-657, 2022.
Available online at www.jafmonline.net, ISSN 1735-3572, EISSN 1735-3645.
https://doi.org/10.47176/jafm.15.03.33300

Method of Improving Stability of a Highly-Loaded Axial Compressor Stage by Coupling Different Casing Treatments

Y. Chen†, A. Lin, H. Zhang and W. Chu

School of Power and Energy, Northwestern Polytechnical University，Xi'an，Shaanxi，710072，China

†*Corresponding Author Email:xjtu.chenyan@nwpu.edu.cn*

(Received August 21, 2021; accepted November 7, 2021)

ABSTRACT

Casing treatment is a powerful method for improving the stability of aircraft compressors. An optimized slot-type casing treatment was tested on the first rotor of a highly-loaded two-stage compressor, and the results showed that the casing treatment could not increase the compressor stability at the design and off-design speeds. A coupled casing treatment (CCT), which is built with an injector, a bridge, a plenum chamber, and several slots for a recirculating loop, is proposed and optimized to enhance the stability of the compressor in the present study. The optimized CCT improves the compressor stability and efficiency under the design condition by 75.8 % and 0.71%, respectively. The coupling effect, which is established with an inner circulation in the slots and an outer circulation from the slots to the injectors, accounts for the excellent stability enhancement. The coupling effect reduces the amount of tip leakage flow, depresses the development of the tip leakage vortex (TLV), and greatly decreases the blockage in the rotor tip which is primarily induced by the interaction of the shock-wave and boundary-layer at the blade suction surface. The parametric study shows that improving the coupling effect has a positive effect on reducing the rotor tip blockage, but a negative effect on the stability of the compressor stage. This is because the inflow condition of the stator is tremendously distorted while the coupling effect is excessively strong, which can cause a stall in the stator rather than in the rotor. The compressor stability can be maximally enhanced by adjusting the strength of the coupling effect to make a compromise of the improved rotor tip flow and the deteriorated stator flow.

Keywords: Aircraft compressor stage; Stall; Coupled casing treatment; Stator corner stall; Stability improvement.

NOMENCLATURE

Ca	axial chord length	*V*	absolute velocity
CCT	Coupled Casing Treatment	*Vz*	axial component of absolute velocity
IGV	Inlet Guide Vane	*Z*	axial direction
LE	Leading Edge	*Za*	slot axial location
N	slot numbers	α	skewed angle in the circumferential direction
R	radial direction	β	lean angle in the axial direction
SMI(s)	Stall Margin Improvement(s)	σ	standard deviations
SC	Solid Casing	Δ	relative change of any parameter
T	blade passing period	ρ	density
TE	Trailing Edge	δar	displacement thickness
TLV	Tip Leakage Vortex	η	compressor efficiency

1. INTRODUCTION

Safe operation of aero engines requires sufficient stall margins of aircraft compressors. However, the compressors tend to stall when encountering inlet distortions, shaft speed variations, and throttle transients. To avoid potential engine failure and aviation accidents, the stall margin should be

extended when designing a compressor. The stall-limited region is usually designed to be located in the rotor tip for typical well-designed modern compressors, through which casing treatments, such as slots, grooves, and tip injection, can be implemented to postpone the occurrence of stall (Hathaway 2007).

Casing treatments have been applied to several well-known aero engines, including CF56, АЛ-31Ф, and WP-14 (Sun *et al.* 2019). However, many other aero engines cannot use casing treatments to improve stability because of two main reasons. One is the efficiency degradation resulting from the application of casing treatments, which causes engine running to be uneconomical. The other is the weak robustness of such treatments in improving stability, which may cause the failure of casing treatments in improving compressor stability when stall styles vary under different operating conditions. Consequently, different endwall treatment technologies, such as slot-type (Wilke *et al.* 2005; Voges *et al.* 2013) and groove-type (Hah 2019; Shabbir and Adamczyk 2005). casing treatments, and tip injection (Suder *et al.* 2000; Taghavi-Zenouz *et al.* 2018), were proposed to make a compromise between the safe operation and fuel economy.

The problem of efficiency degradation has been studied and discussed extensively. Lin *et al.* (2018, 2019) proposed a feasible method of injecting water mist into the air to improve the compressor performance of gas turbines. Fujita and Takata (1987) tested different axial, skewed and circumferential groove casing treatments and concluded that the greater the effectiveness of casing treatments in improving stability, the greater is the efficiency penalty. Lu *et al.* (2006), *Alone et al.* (2017) and Brignole *et al.* (2008) optimized bend skewed slots and semicircular slots to minimize the efficiency degradation, respectively. Goinis *et al.*(2013) used an automated multi-objective optimization procedure to optimize slots. Cumpsty *et al.* (1989) made the casing treatment cover partially the annulus for reducing the efficiency loss. Wang *et al.*(2014) proposed alternative methods or criteria to minimize the design and optimization time. Another method of reducing the performance degradation involves implementing an active stall control system to develop a smart engine (Epstein 1985), passive tip injection (Suder et al. 2000; Dinh *et al.* 2015), recirculating casing treatment (He and Zheng 2019), and new-type endwall technologies such as SPS casing treatment (Sun *et al.* 2019), plasma actuation (Zhang *et al.* 2019), labyrinth casing (Mileshin *et al.* 2018), and combined configurations((Dinh *et al.* 2015; Halawa *et al.* 2015). Several of the above works have been very successful, but obtaining an adequate stall margin with the least performance degradation remains highly challenging.

Most studies focused on the successful application of casing treatments and their relative mechanisms. Moreover, a better in aerodynamic performance is of concern in design and optimization (Liu *et al.* 2021-a, and 2021-b). Nevertheless, the casing treatment tends to fail in improving stability when the working conditions, quantities such as shaft speed (Wilke *et al.* 2005), tip clearance (Rolfes *et al.*2017), and inlet condition (Sun *et al.* 2018) change. Greitzer *et al.* (1979) and Cheng *et al.* (1984) found that the effectiveness of a casing treatment depends on blade solidity. It is necessary to conduct a numerical analysis to get more information on the flow field (Lin *et al.* 2021-a; Liu *et al.* 2021-c). Wilke *et al.* (2005) found that the casing treatment is effective in improving stability at 100% of the design speed by numerical analysis, but fails at 60% of the design speed. Moreover, tip injection cannot function unless the injected mass flow is more than 2% of the compressor annulus flow (Hiller *et al.* 2011) in a stage environment, which is different from that in an isolated rotor environment (Li *et al.* 2015). The failure of the casing treatments is primarily because the improvement of compressor stability is closely related to the manipulation of the tip leakage vortex (TLV), which is discussed by Wilke *et al.* (2005), Voges *et al.* (2013), and Lu *et al.* (2006) and Schnell *et al.* (2011) and Lu *et al.* (2006) in detail. The casing treatment may fail in improving stability once the compressor stall mechanism alters. Heinichen *et al.* (2011) concluded that casing treatment can effectively improve compressor stability given that the compressors stall is triggered by the TLV.

In the present, little effort has been paid to the stall control of the compressor whose stall is not triggered by the TLV concerning the casing treatment. Whether the casing treatment can suppress stall induced by boundary-layer separation is not disclosed. Wang *et al.* found that a slot-type casing treatment fails to enhance the stability of a highly-loaded compressor stage because the stall is mainly caused by the interaction of the passage shock-wave and boundary layer, but not the TLV (Wang *et al.* 2020). Consequently, in the present study, a new-type coupled casing treatment (CCT) is proposed and optimized to stabilize the compressor. The idea is derived from the experimental results that the stability of the compressor equipped with a groove-type casing treatment can be further improved by implementing tip injection (Wang *et al.*2017). If the CCT can manipulate the shock-wave induced boundary-layer separation, it provides a potential for solving the problem of weak robustness of casing treatments.

Included here is a systematic study of the coupling method in the compressor stage. This article begins by investigating the effects of CCT geometric parameters on the compressor performance to build an optimal structure. This is followed by the mechanism study of the obtained stability enhancement. In addition, the unsteady flow characteristics and the stall dynamic of the compressor equipped with a CCT are lastly discussed.

2. DESIGN OF CCT

2.1 Geometric structure

The CCT was designed based on the understanding of the effects and characteristics of different endwall-treatment technologies (Wang *et al.*2017; Wang *et al.*2018; Lu *et al.*2007). The CCT was composed of an injector, a bridge, a plenum chamber, and several slots for a blade passage, which is presented in 0. The slots were employed to build an inner flow circulation for reducing tip blockage induced by the TLV and bleed low-energy fluid caused by boundary-layer separation. The plenum chamber was used to balance the pressure among the slots for reducing pressure fluctuations in the blade passage (Wang *et al.* 2015) induced by the installed endwall treatment and collect air extracted from the slots. Another objective of setting up the plenum chamber was to transport local serious blockage induced by potential inlet distortions along the circumferential direction. Tip injection that was implemented with the injector was to energize the TLV and excite the annulus boundary layer near the shroud. The injector was placed in the passage of the inlet guide vane (IGV) along the direction of the main flow. The bridge was employed to connect the injector and the plenum chamber.

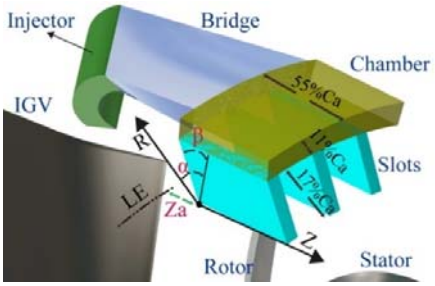

Fig. 1. Geometric structure of coupled casing treatment.

2.2 Parametric geometry

The CCT structure was geometrically parameterized with slot axial location Za, numbers *N*, skewed angle α in the circumferential direction, and lean angle β in the axial direction. The studied variables are given in Table 1. To study the effect of a geometrical parameter, the values of the other variables were fixed. The geometrical parameters that were not investigated were determined by the design experience of each part. The slot axial length was 55% of the blade chord length (Ca), which was the same as the slot-type casing treatment which was proven ineffective in enhancing stability (Wang *et al.* 2020). The radial heights of the slots and the plenum chamber were 17% Ca and 11% Ca respectively, which were determined with the results in the literature (Wang *et al.* 2015). The total radial height of the slots and plenum chamber was equal to that of the slot-type casing treatment. The open width of a slot occupied 8.3% of one blade pitch, and the open porosity varied with the slot numbers. The injector throat height and circumferential coverage were set to be six times the tip clearance size and 67% respectively, which was determined based on parametric studies of the injector size in literature (Wang *et al.* 2017).

3. Investigated compressor

The first stage of a two-stage highly loaded axial compressor was used to evaluate the CCT. The blade numbers of the inlet guide vane (IGV), rotor 1, and stator 1 are 21, 17, and 50, respectively. The design speed was 12100 rpm and the relative Mach number is 1.8 at the rotor tip. The running rotor tip clearance size was 0.6 mm. The geometric angles of the IGV changed with speed according to a vane schedule, and the angle was bound as 18° at 90% of the design speed. An optimized slot-type casing treatment was found to be ineffective in improving stability at 90% of the design speed because the compressor stall was not triggered by the TLV. The compressor stall mechanism was discussed in detail in Wang *et al.*2020. Figure 2 demonstrates the compressor maps for the two-stage compressor with and without the slot-type casing treatment. The CCT in this paper is proposed to extend the stable operating range stability and studied at 90% of the design speed.

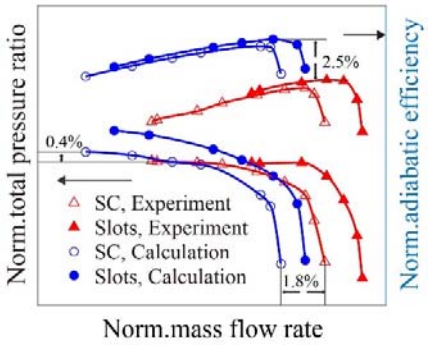

Fig. 2. Comparison of compressor characteristics between the solid casing and casing treatment at 90% of design speed.

Table 1 Studied geometric parameters of coupled casing treatment

Variable	Value				Fixed value
Za /Ca	-13.9	0	13.1	30.7	α=45º, β=0 º, N=9
α / º	0	30	45	60	Za =13.1Ca , β=0 º, N=9
β / º	0	45	60	75	Za =13.1Ca, α=45º, N=9
N / º	1	3	5	9	Za =13.1Ca, α=45º, β=45º, N=9

3. NUMERICAL METHODOLOGY AND VALIDATION

3.1 Numerical methodology

We used a commercial CFD package NUMECA FINE/Turbo to investigate the effect of the CCT on the compressor stage. The equations were discretized in space with a second-order upstream finite-volume formulation. The one equation turbulence model, namely, Spalart and Allmaras, was employed to estimate the eddy viscosity. The viscous fluxes were evaluated in a central differencing manner with Gauss theorem. The Reynolds-averaged Navier–Stokes (RANS) calculations were implemented to carry out the parametric study of the CCT, and the time-accurate RANS simulations were carried out to understand the flow details. In the time-accurate simulations, the blade numbers of the IGV and stator were changed to 17 and 51, respectively, to meet the requirement of identical circumferential coverage of interfaces. Three blade passages of the stator were used to match the rotor passage. Temporal integration was implemented using the implicit pseudo-time scheme. The physical time steps numbered 153 for a single blade passage with a total of 20 pseudo-time interactions.

The fluid was defined as a perfect gas with a constant isentropic coefficient and heat capacity. A constant total pressure (45,700 Pa) and total temperature (288.2 K) were implemented at the inlet boundary. The average static pressure was varied at the outlet boundary to obtain different operating points with an accuracy of 500 Pa when approaching the stall limit. Adiabatic and nonslip conditions were imposed on all solid walls.

Figure 3 depicts the grid topology of all the blade passages. The blade passages of the IGV and stator 1were modeled with the O4H topology. The inlet and outlet used H-blocks and the blade used O-blocks. The IGV passage consisted of 65 pitch-wise, 73 spanwise, and 109 streamwise points, and the stator passage included 69 pitch-wise, 89 spanwise, and 113 streamwise points. The rotor blade passage was surrounded with an O-block including 369 gird numbers. The rotor tip clearance was meshed using the butterfly topology with 25 points in the radial direction. The mesh was stretched toward all solid boundaries to meet the resolution requirement of $y+\leq 2$ owning to the use of low-Reynolds estimation of the boundary layer in the used turbulence model (Lin *et al*. 2021-b). The plenum chamber, bridge, and injector were modeled with H blocks, consisting of 85×25×109, 85×25×45, 85×25×85 cells in spanwise, pitch-wise, and streamwise directions, respectively. The total mesh of the compressor stage and the CCT consisting of 23 blocks contained approximately 4,270,000 grid points.

3.2 Validation

The validation of the numerical model was carried out for the two-stage compressor because the first

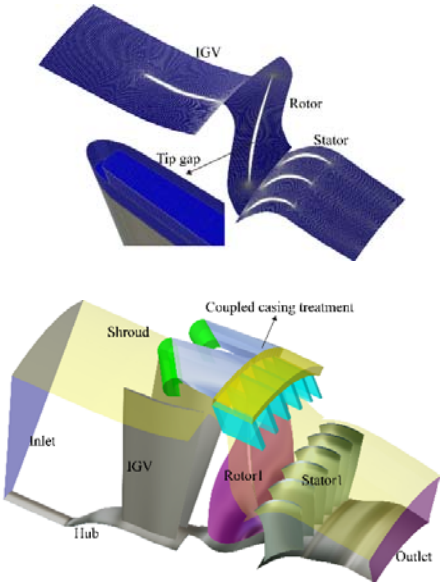

Fig. 3. Computational grid description of compressor used.

stage was not tested separately. As shown in Fig. 2, the choked mass flow rates are underestimated, and the total pressure ratio agrees reasonably with the experimental results. The compressor efficiency is overestimated, which is probably results from the incapability of the turbulence model in predicting the rise in temperature in the blade passage (Hah 2015). Lurie and Breeze-Stringfellow (2015) and Yang *et al*. (2020) also found the discrepancy in compressor efficiency between the experimental and calculation results for another highly loaded compressor. In general, the numerical model used captures the trend of compressor characteristics and the primary influence of the tested slot-type casing treatment.

To check the predicting ability of the numerical model for the studied stage, the total pressure ratio along the span is shown in 0 for the first stage. The calculated total pressure ratio agrees well with the experimental result. A marginal discrepancy can

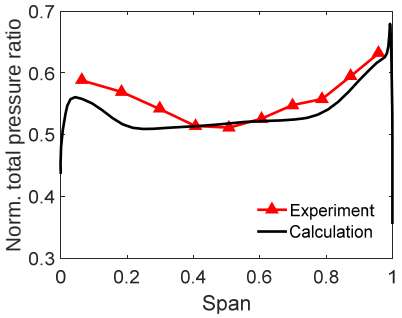

Fig. 4. Radial profile of total pressure ratio under near-stall condition for the compressor first stage.

be found near the hub, which was observed for the transonic compressor of NASA ROTOR 37 as well (Denton 1993). This discrepancy is probably caused by the penetration of probes in a relatively limited space near the hub, resulting in relatively larger measurement errors.

4. Results And Discussion

4.1Effect on compressor performance

Figure 5 displays compressor characteristics of the solid casing, slot-type casing treatment, and CCTs with different slot numbers at 90% of the design speed. All the results are derived from the time-accurate simulations. The slot axial location Za, skewed angle α, and lean angle β are set to be 13.1% Ca, 45ºand 45º, respectively. The CCT geometric parameters are determined by compromising the compressor stability and efficiency using the results in Fig.6. Stall margin improvement (SMI) is evaluated by the change of stable operating range

$$\mathrm{SMI} = \left[\frac{m_{\text{peak efficiency,CCT}} - m_{\text{stall,CCT}}}{m_{\text{peak efficiency,SC}} - m_{\text{stall,SC}}} - 1\right] 100\% \qquad (1)$$

The change of efficiency $(\Delta\eta)$ is defined by the efficiency difference between the CCTs and the solid casing under the operating condition of peak efficiency

$$\Delta\eta = \eta_{\text{peak efficiency,CCT}} - \eta_{\text{peak efficiency ,SC}} \qquad (2)$$

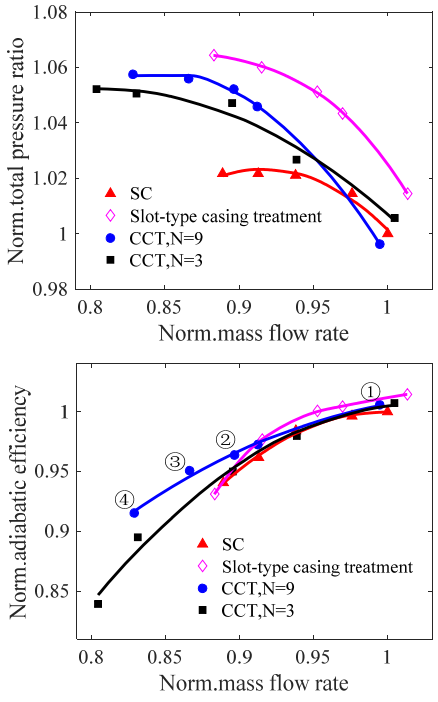

Fig. 5. Performance maps of compressors with different casing treatments.

Compared with the solid casing, the CCTs with 9 and 3 slots improve compressor stability by 49.5% and 75.8% respectively, and improve the compressor efficiency by 0.54% and 0.71% respectively. The choked mass flow rate is not remarkably changed by the CCTs. Compared with the slot-type casing treatment, the compressor efficiency, total pressure ratio, and choked mass flow rate are slightly decreased, but the stall margin is improved significantly by the CCTs. Consequently, the proposed CCT is capable of enhancing the compressor stability and efficiency simultaneously. The following part is to implement parametric studies for understanding the effective mechanisms.

4.2 Effects of CCT geometric parameters

The effects of different CCTs on compressor stability and efficiency are focused on in the section. 0 6 depicts the SMI and Δη for the compressor equipped with different CCTs. The other CCT parameters are fixed when studying the effect of one geometric parameter, as shown in Table 1. The slot location has a great effect on the compressor performance, which is given in 0 (a). The SMI improves with the slots shifted downstream, but decreases slightly while the value reaches up to be 30.7%Ca. The compressor efficiency decreases constantly when shifting the slots towards the downstream direction. Figure 6 (b) shows the effect of slot skewed angle on the compressor performance. The slot skewed angle is an extremely important factor when designing a slot-type casing treatment, which is the same as the CCT design. The skewing of the slots helps bleed air from the blade passages to the casing treatment. The SMI is maximized when the skewed angle is equal to be 45°, and the compressor efficiency improves with the skewed angle increased. The configuration with a larger skewed angle is not calculated because the orthogonality of the grid cells near the circular casing gets deteriorated. As illustrated in 0 (c), the increase of the slot lean angle contributes to improving the compressor efficiency when the angle is lower than 60° but leads to the decrease of SMI. The optimal slot number is equal to be 3 for improving the compressor stability and efficiency, which is different from that in the slot-type casing treatment.

In summary, the studied CCT geometric parameters have significant effects on compressor performance. Based on the understanding of the compromise of compressor stability and efficiency, the configuration (Za =13.1Ca, α=45º, β=45º, N=3) is regarded as the optimal structure for improving the compressor performance. Another configuration with the slot number of 9, as shown in 0, is also selected to implement time-accurate calculations for comparison. The following part will focus on the effect of the slot axial location on the compressor flow for understanding the relative mechanisms because this character influences both the stability and the efficiency remarkably.

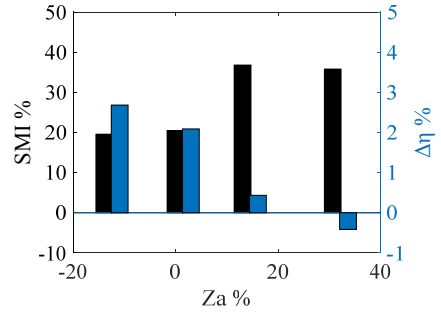

(a) Effects of slot axial location

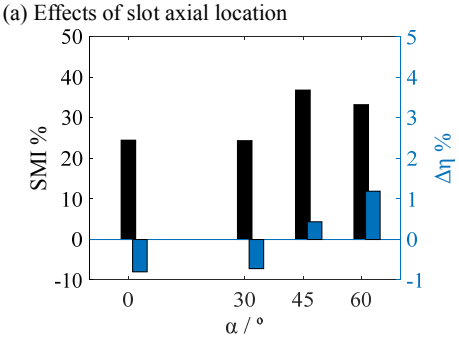

(b) Effects of slot skewed angle

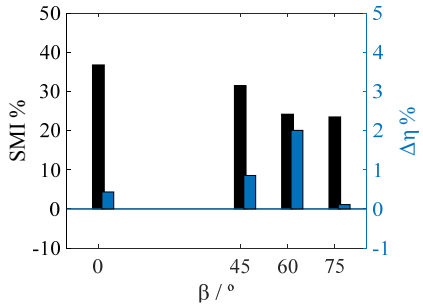

(c) Effects of slot lean angle

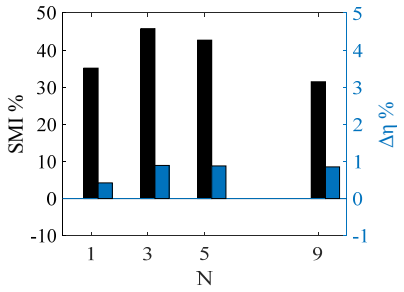

(d) Effects of slot numbers

Fig. 6. Changes of the compressor stability and efficiency with CCTs implemented.

Figure 7 depicts the distributions of the TLV colored with relative velocity and reversed flow regions (Vz<0) represented by grey zones along 99% span under the near stall condition for the SC and CCTs. Displacement thickness (δar) (Wang *et al.* 2019) of the axially reversed flow, which can capture the blockage induced by both the TLV and the separated boundary layer, is adopted to quantify the tip blockage (0).

In the SC, a large blockage zone is formed by the interaction of the TLV, boundary layer, and passage shock wave (Wang *et al.* 2020). Compared with SC, the TLV is greatly depressed by the CCT when the axial location Za is equal to be -13.9%Ca. The break off of the streamlines is caused by the absorption of the CCT. As the slots move to the location of 30.7%Ca, the TLV-induced blockage enhances but it does not stretch across the blade passage as that in the solid casing. The blockage near the blade trailing edge is also increased owing to the boundary-layer separation at the blade suction surface. The blockage is even greater than that in the solid casing on an observation of the displacement thickness in Fig. 8. The increased tip blockage does not decrease the SMI (Fig. 6). On the contrary, the SMI improves with the slots shifted downstream. Moreover, the compressor efficiency decreases continuously with the slots shifted downstream.

By comparing the SMIs (0) and the quantitative values of tip blockage (0), it can be found that

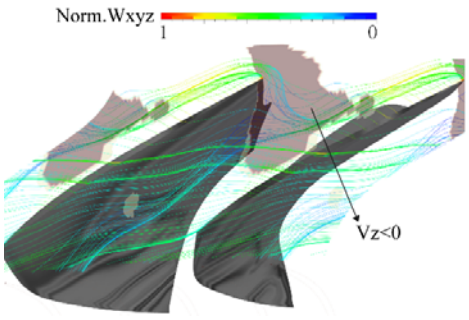

(a) SC

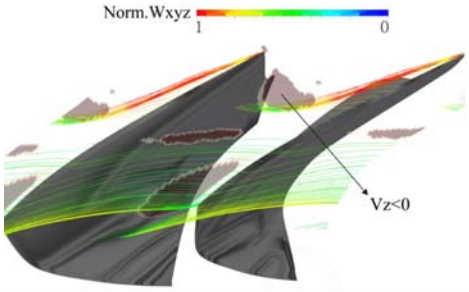

(b) CCT, Za = -13.9%Ca

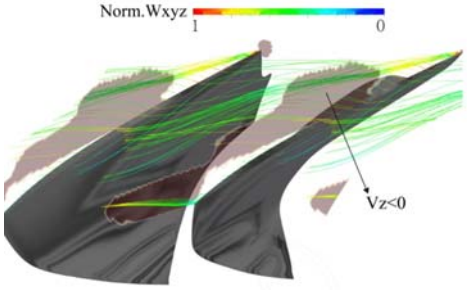

(c) CCT, Za = 30.7%Ca

Fig. 7. Distributions of tip leakage flow and reversed flow region for the CCTs and SC.

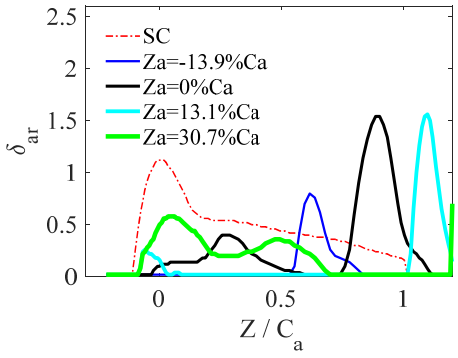

Fig. 8. Displacement thickness along the axial direction for the CCTs and SC.

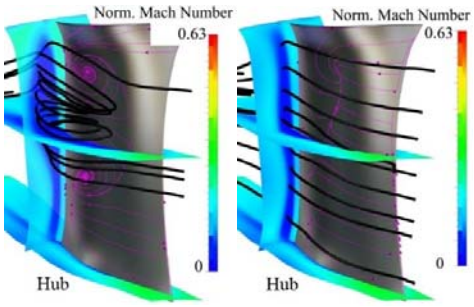

(a) Za = -13.9%Ca (b) Za = 30.7%Ca

Fig. 9. Distributions of streamlines and Mach number for the CCTs with different axial locations.

the compressor stability is not closely related to the decrease of tip blockage. Furthermore, the tip blockage under the effect of CCTs is too limited to induce compressor stall. There must be some other reasons that may trigger the stall of the compressor stage.

Figure 9 presents the distributions of limiting streamlines on the suction surface of the stator, 3D streamlines, and the Mach number at the stator outlet. For the CCT with Za = -13.9%Ca, the air near the shroud and the hub moves towards the blade middle section along the radial direction and interacts with the local boundary layer, resulting in two focuses on the blade suction surface. A shedding vortex is thus formed, which causes a large low-velocity zone at the stator outlet, occupying nearly 50% span. The flow conditions in the stator have much more deteriorated than that in the rotor, which implies that the stator is probably a new factor that triggers compressor stall. While the slots shift to the location of 30.7%Ca, only a separation line can be found at the rear part of the blade, and the induced low-velocity zone is nearly uniformly distributed along the whole span. Consequently, shifting the slots downstream can weaken the influence of the CCTs on the stator flow, which may account for the SMI trend that is shown in 0 (a).

The tremendous flow difference among the stators must result from the flow redistributions caused by installing the CCTs. To analyze the flow redistributions quantitatively, the mass flow is azimuthally averaged and normalized with an arbitrary value. The relative changes of mass flow between the CCTs and the solid casing are calculated on the meridianal plane under the condition of point ②, which is shown in 0. The discharging capacity in the rotor tip is greatly improved owing to the CCTs, which is consistent with the reduction of the reversed flow zone, as shown in 0. The trace of the increased mass flow in the rotor penetrates into the stator, resulting in a huge flow variation in the upper 50% span when the slots are located upstream of 0% Ca. The effect is weakened as the slots shift towards the downstream direction, which is responsible for the disappearing of the shedding vortex (0). It seems that the greater the effectiveness of the CCTs in reducing the rotor tip blockage, the greater is the flow redistributions in the stator.

Based on the results above, the enhancement of compressor stability must be a compromise of the flow improvement in the rotor tip and the flow deterioration in the stator. The former benefits from the flow transport built in the CCT, which will be

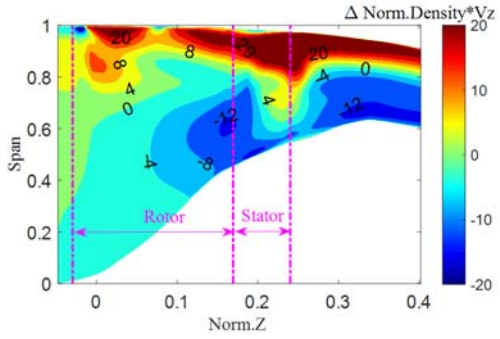

(a) Za = -13.9%Ca

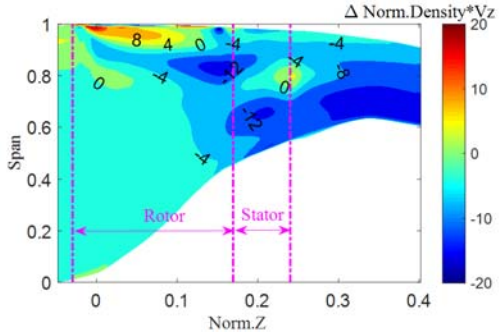

(b) Za = 30.7%Ca

Fig. 10. Relative changes of mass flow between the CCTs and the solid casing at the near stall condition.

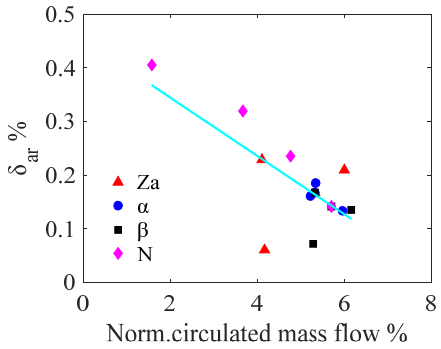

Fig. 11. Changes of averaged displacement thickness with circulated mass flow rates.

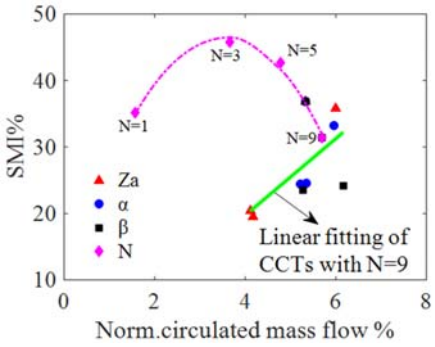

Fig. 12. Changes of stall margin improvements with circulated mass flow rates.

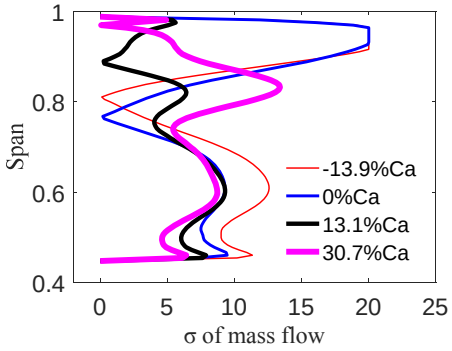

Fig. 13. Radial distributions of standard deviations of mass flow for the CCTs.

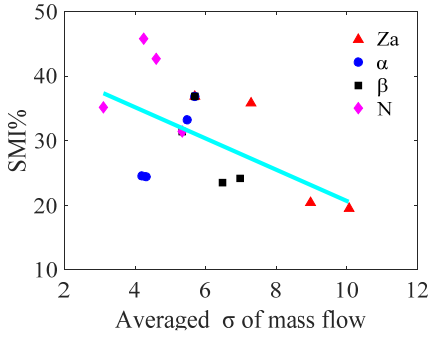

Fig. 14. Relationship between stall margin improvements and inflow distortions at the stator inlet.

analyzed in the next section. The effectiveness of CCTs in reducing the tip blockage, defined as a coupling effect, is evaluated with the circulated mass flow rate from the plenum chamber to the injector. The displacement thickness is averaged along the axial direction using the data in 0. Figure 11 demonstrates the relationship between the circulated mass flow rates and the average displacement thickness. The fitted line indicates that improving the coupling effect has a positive effect on the decrease of tip blockage.

The relationship between the coupling effect (represented with the circulated mass flow rate) and the SMIs is presented in 0. When the slot numbers are 9, the fitting (represented by a solid line) between the coupling effect and SMIs is linear, which implies that the gain of the coupling effect generally leads to an increasing trend of compressor stability. However, a peak appears on the fitted curve (dashed line) for the CCTs with different slot numbers. Increasing the slot numbers will definitely lead to the enhancement of the coupling effect and thus the reduction of tip blockage. Therefore, the decrease of SMI probably is caused by the flow deterioration in the stator while the slot numbers are larger than 3.

The influence of CCTs on the stator can be calculated with the flow distortion at the stator inlet. Based on the results in 0, the standard deviations (σ) of the mass flow changes at the stator inlet are calculated and shown in 0 for the CCTs with different axial locations. The SMI improves with the slots shifted downstream, but decreases slightly while the value reaches up to be 30.7%Ca. The downstream shifting of CCTs reduces the low distortion at the stator inlet, especially at a higher span, which leads to the increase of SMI in Fig.6 (a).

The σ is then averaged along the whole span, and the relationship between the SMIs and the averaged σ for all the CCTs is depicted in 0. The increased distortion at the stator inlet generally caused the decrease of the SMIs. This trend confirms that the flow deterioration in the stator is responsible for the decay of SMIs. The accuracy of the fitted curves in 0 and 0 is relatively low because the compressor stability is determined by both the flow improvement in the rotor tip and the flow deterioration in the stator.

In summary, the CCT causes significant changes in the flow in the rotor and stator. Compressor stability in a staging environment is not only determined by the decrease of the rotor tip blockage but also by the increase of the stator inlet distortion which is induced by the casing treatment. This is different from the design of a casing treatment in a rotor-isolated environment. To maximize the SMI, the optimal CCT should dampen the tip blockage in the rotor as much as possible and minimize the influence on the

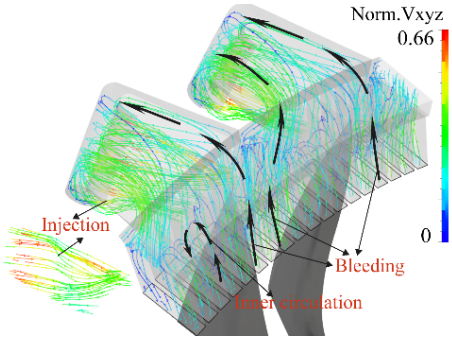

Fig. 15. Instantaneous distributions of streamlines in the CCT with N=9.

stator simultaneously. Conversely, the stator should be designed under the effect of the casing treatment.

4.3 Mechanism of stability enhancement

We will discuss the flow details in the CCT and the influence on the blade passage flow for understanding the underlying mechanism of stability enhancement. The following discussion focus on the operating condition corresponding to the stall limit of the solid casing (point ②), namely, all the results in this section are compared at the same mass flow.

Figure 15 shows the distributions of the streamlines in a recirculating loop for the CCT with slot number =9. An inner circulation is formed as expected for the slots that stretch over the rotor blade. Most of the flow is bled into the slots and travels into the plenum chamber, and then turns out to be the air source of tip injection. This forms an outer circulation. The two circulations are responsible for any benefits of the compressor performance.

Figure 16 depicts the instantaneous distributions of the relative Mach number, reversed flow regions, and streamlines of the TLV for the CCT with N = 9. The CCT greatly depresses the development of the TLV, resulting in a very small zone of blockage near the blade suction surface. The circumferential propagation of the double-leakage flow is mostly cut off. The injection trace can be clearly observed in the IGV passage. The jet helps to energize the annulus boundary layer, which reduces the attack angle of the rotor inlet. The low-velocity part at the left bottom of the injector is caused by the high pressure behind the shock wave. The influence of the CCT with N = 3 (not shown) is nearly the same. Therefore, the flow circulations significantly improve the flow condition of the rotor tip.

Figure 17 illustrates the unsteady changes of the displacement thickness (δ_{ar}) as a function of the blade passing period (T) under different operation conditions. The operating conditions derived from Fig.5 are marked on the graphs. The unsteady variation of δ_{ar} for the solid casing under the condition ② is also shown for comparison.

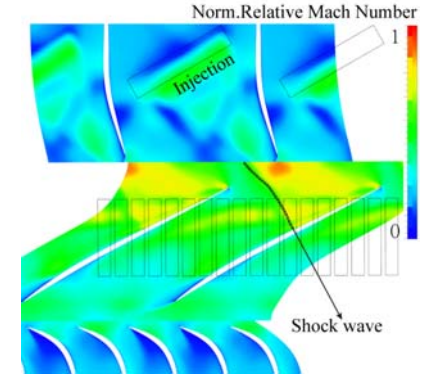

(a) Relative Mach number

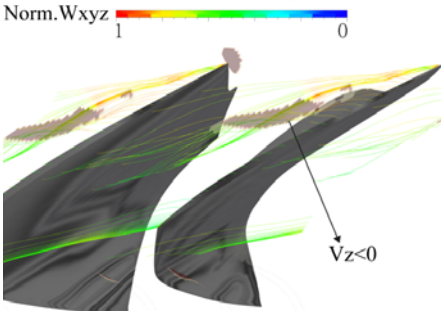

(b) Tip leakage flow and reversed flow region

Fig. 16. Instantaneous flow distributions alone 99% span for the CCT with N=9.

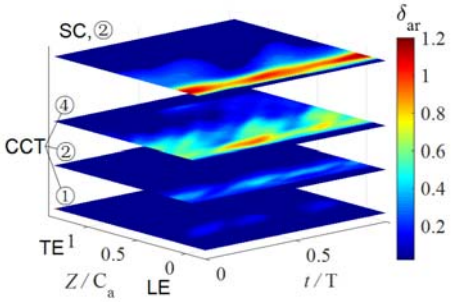

(a) CCT with N=3

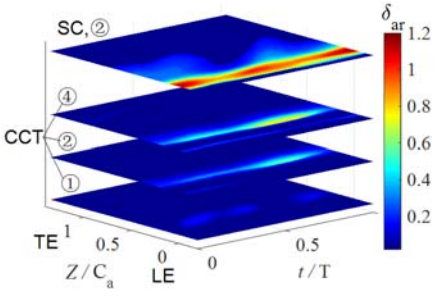

(b) CCT with N=9

Fig. 17. Fluctuations of azimuthal-averaged displacement thickness with time at different operating conditions.

The blockage at the rotor tip increases when the compressor is throttled for the CCTs. The blockage is significantly reduced for the CCTs compared to that in the solid casing by comparing the working conditions ②, and the unsteadiness of the tip blockage is greatly decreased as well. As the compressor operates to the stall limit (④) of the CCT, the displacement thickness explodes for the CCT with 3 slots due to the weaker coupling effect, which is completely opposite to that in the CCT with 9 slots. This implies that the compressor stall under the effect of different CCTs may be triggered by different factors.

Given that the compressor stall without a CCT is triggered by both the TLV and shock-induced boundary-layer separation, the unsteady characters of the tip leakage intensity and blade tip loading are compared in 0 for the solid casing and the CCTs under the operating condition ②. The tip leakage intensity is represented by the mass flow in the middle section of the tip gap along the radial direction, and the blade tip loading is calculated using the pressure difference between the pressure surface and the suction surface.

The tip leakage flow in the solid casing is totally unsteady, and the unsteadiness is dampened by the CCTs. Compared with the solid casing, the time-averaged leakage intensity is reduced by approximately 38% and 42% by the CCTs with 3 slots and 9 slots, respectively, which implies that the effect on the tip leakage is similar for the CCTs with different slot numbers. Therefore, the manipulation of TLV helps to depress stall, but and is not responsible for the different SMIs between the two CCTs.

The spike of the blade tip loading in 0 (b) can represent the location of the shockwave. The shock wave is located at 24%Ca from the blade leading edge (LE). The shock wave is pushed downstream to 32%Ca and 37%Ca by the CCTs with 3 slots and 9 slots, respectively. The time-averaged blade tip loading is increased by approximately 21% by the two CCTs. The trace of the increased loading due to the slots can be clearly identified in the CCT with 3 slots. The blade loading upstream of the shock wave in the CCT is lower than that in the solid casing resulting from the injection effect (0). This effect can weaken the strength of the shock wave and then reduce the bounder-layer separation. For the part downstream of the shock wave, the blade loading is enhanced due to the manipulation of the secondary flow.

The CCT with N=9 is used to understand the stall mechanism induced by the stator. The instantaneous distributions of streamlines in the stator and the relative Mach number are shown in Fig. 19 under the stall limit condition. The flow characteristics are not the same in different blade passages, but the shedding vortex can be found near the hub of all the blade passages. The corner vortex explodes to block.

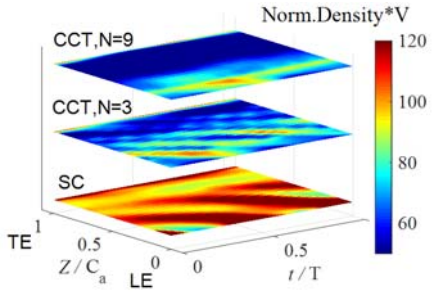

(a) Tip leakage intensity through the tip gap

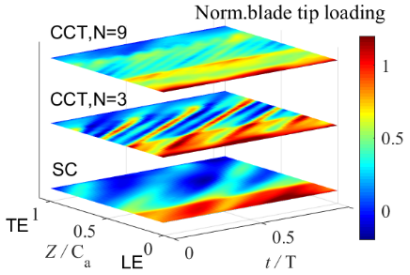

(b) Blade tip loading

Fig. 18. Comparison of unsteady flow characteristics between the solid casing and the CCTs under the near stall condition.

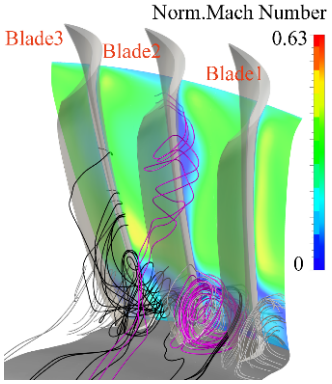

Fig. 19. Instantaneous flow distributions in the stator under the stall limit condition.

the whole blade passages below 25% span and is responsible for the stall of the compressor stage equipped with the CCT when the rotor tip does not trigger stall

In conclusion, two circulations, namely, the slot inner circulation and the outer circulation from the slots to the injectors, are formed in the CCT, forming the coupling effect. This coupling effect reduces the tip leakage intensity, depresses the development of the TLV, and decrease greatly the boundary-layer separation induced by the shock wave. These effects successfully eliminate the tip blockage in the rotor

blade passage, resulting in the remarkable improvement of compressor stability. The strength of the coupling effect is closely related to the geometry of the CCT, and different CCTs may cause different stall mechanisms.

5. CONCLUSION

In order to depressor the stall induced by both the boundary-layer separation and TLV in a compressor stage, a coupled casing treatment is proposed based on the understanding of the characteristics of various endwall treatments. Slots, a plenum chamber, a bridge, and an injector were employed to build the CCT, and parametric studies were implemented to optimize the configuration. The time-accurate simulations were carried out to explore the flow mechanism of stability enhancement and the stall mechanism of the compressor stage equipped with the CCTs.

The optimal CCT improves the stability of the compressor stage by 75.8% and the compressor efficiency by 0.71% under the design point. The CCT manifests itself as a method of tremendous potential for improving compressor performance. The location and number of the slots have a greater effect on the compressor stability than the other geometric parameters.

The coupling effect is established by an inner circulation in the slots and an outer circulation from the slots to the injectors in the CCT. The coupling effect reduces the amount of the tip leakage flow, depresses the development of the TLV, and greatly decreases the boundary-layer separation induced by the shock wave, resulting in enhanced compressor stability. The parametric result concludes that the increase of the coupling effect has a positive effect on the decrease of rotor tip blockage, but not on the enhancement of compressor stability.

The CCT causes intense flow redistributes in the radial direction, and the stronger the coupling effect, the greater is the flow distortion at the stator inlet. The increase of the inlet distortion is detrimental to the stage stability. The maximum stability enhancement is obtained on the condition that the tip blockage at the rotor tip is effectively depressed and the stator inlet distortion is kept within a certain limit.

REFERENCES

Alone D. B., Kumar S. S., Shobhavathy M. T., Mudipalli J. R. R., Pradeep A. M., Ramamurthy S., Venkat S. I. (2017). Experimental assessment on effect of lower porosities of bend skewed casing treatment on the performance of high-speed compressor stage with tip critical rotor characteristics. *Aerospace Science and Technology* 60,193-202.

Brignole, G. A., Danner F. C. T and H. P. Kau (2008). Time resolved simulation and experimental validation of the flow in axial slot casing treatments for transonic axial compressors. *ASME Turbo Expo 2008* : Berlin , Germany , *363-374.*

Cheng, P., M. E. Prell, E. M. Greitzer and C. S. Tan (1984). Effects of Compressor Hub Treatment on Stator Stall and Pressure Rise. *AIAA Journal of Aircraft* 21 (7),469–475.

Cumpsty, N. A. (1989). Part-circumference casing treatment and the effect on compressor stall. *ASME Turbo Expo 1989*. American Society of Mechanical Engineers.

Denton, J. D. (1993). Loss Mechanisms in Turbomachines. *Journal of Turbomachinery* 115(4), 621-656.

Dinh, C. T, M. W. Heo and K. Y. Kim (2015). Aerodynamic performance of transonic axial compressor with a casing groove combined with blade tip injection and ejection. *Aerospace Science and Technology* 46,176-187.

Epstein, A. H. (1985). 'Smart' engine components - A micro in every blade. *AIAA Paper AIAA-85-1296*.

Fujita, H. and H. Takata (1987). A Study on Configurations of Casing Treatment for Axial Flow Compressors. *Bulletin of the JSME* 27 (230) ,1675-1681.

Goinis, G., V. Christian and A. Marcel (2013). Automated optimization of an axial-slot type casing treatment for a transonic compressor. *ASME Turbo Expo 2013*. Turbine Technical Conference and Exposition.

Greitzer, E. M., J. P. Nikkanen, D. E. Haddad, R. S. Mazzawy and H. D. Joslyn (1979). A Fundamental Criterion for the Application of Rotor Casing Treatment. *Journal of Fluids Engineering* 101(2), 237–243.

Hah, C. (2015). Effects of Unsteady Flow Interactions on the Performance of a Highly-loaded Transonic Compressor Stage. *ASME Turbo Expo 2015*, Turbine Technical Conference and Exposition.

Hah, C. (2019). The inner workings of axial casing grooves in a one and a half stage axial compressor with a large rotor tip gap: Changes in stall margin and efficiency. *Journal of Turbomachinery* 141(1),1-16.

Halawa, T., M. Alqaradawi, O. Badr and M. S. Gadala (2015). Numerical simulation of using combined active and passive stall control techniques in centrifugal compressors. *ASME 2014 International Mechanical Engineering Congress and Exposition, IMECE2014-37983*.

Hathaway, M. D. (2007). Passive Endwall Treatments for Enhancing Stability. *NASA Technical Paper TR-3878*.

He, X. and X. Zheng (2019). Roles and mechanisms of casing treatment on different scales of flow instability in high pressure ratio centrifugal compressors. *Aerospace Science and Technology* 84, 734-746.

Heinichen, F., V. Gummer and H. P. Schiffer (2011). Numerical Investigation of a Single Circumferential Groove Casing Treatment on Three Different Compressor Rotors. *ASME Turbo Expo,* Turbine Technical Conference and Exposition.

Hiller, S. J., R. Matzgeller and W. Horn (2011). Stability enhancement of a multistage compressor by air injection. *Journal of Turbomachinery* 133(3),031009-1- 031009-7.

Li, J., F. Lin, Z. Tong, C. Nie and J. Chen (2015).The Dual Mechanisms and Implementations of Stability Enhancement with Discrete Tip Injection in Axial Flow Compressors. *Journal of Turbomachinery* 137(3),031010-1~031010-10.

Lin, A., Y. Sun, H. Zhang, X. Lin and Lu. Yang (2018). Fluctuating characteristics of air-mist mixture flow with conjugate wall-film motion in a compressor of gas turbine. *Applied Thermal Engineering* 142, 779-792.

Lin, A., Q. Zheng, Y. Jiang, X. Lin and H. Zhang (2019). Sensitivity of air/mist non-equilibrium phase transition cooling to transient characteristics in a compressor of gas turbine. *International Journal of Heat and Mass Transfer* 137, 882-894.

Lin A. Q., Liu G. W., Chen Y., Feng Q., Zhang H. (2021a). Evaluation and analysis of evaporation cooling on thermodynamic and pressure characteristics of intake air in a precooled turbine engine. *International Journal of Hydrogen Energy* 46(47), 24410-24424.

Lin, A., G. Liu, X. Wang and Q. Feng (2021b). Comprehensive evaluations on performance and energy consumption of pre-swirl rotor–stator system in gas turbine engines. *Energy Conversion and Management* 244, 114440.

Liu, G., W. Gong, H. Wu, L. Pang, A. Lin (2021a). Theoretical and experimental evaluation of temperature drop and power consumption in a cover-plate pre-swirl system for gas turbine cooling. *Case Studies in Thermal Engineering* 27, 101221.

Liu, G., X. Wang, W. Gong and A. Lin (2021b). Prediction of the sealing flow effect on the temperature drop characteristics of a pre-swirl system in an aero-engine. *Applied Thermal Engineering* 189, 116717.

Liu, G., W. Gong, H. Wu and A. Lin (2021-c). Experimental and CFD analysis on the pressure ratio and entropy increment in a cover-plate pre-swirl system of gas turbine engine. *Engineering Applications of Computational Fluid Mechanics* 15(1), 476-489.

Lu, X., W. Chu, Y. Zhang and J. Zhu (2006). Experimental and numerical investigation of a subsonic compressor with bend-skewed slot-casing treatment. *Proceedings of the Institution of Mechanical Engineers, Part C: Journal of Mechanical Engineering Science* 220 (12),1785-1796.

Lu, X., W. Chu and J. Zhu (2007). Numerical investigations of the flow mechanisms in a subsonic compressor rotor with axial-skewed slot. *Proceedings of the Institution of Mechanical Engineers, Part A: Journal of Power and Energy* 221 (3),301-313.

Lurie, D. P. and A. Breeze-Stringfellow (2015). Evaluation of Experimental Data From a Highly Loaded Transonic Compressor Stage to Determine Loss Sources. *ASME Turbo Expo 2015*, Turbine Technical Conference and Exposition.

Mileshin, V. I., A. M. Petrovitchev and V. V. Zhdanov (2018). Numerical and experimental investigation as applied to effects of labyrinth-type casing treatments on performance of high-loaded compressor first stage. *ASME Turbo Expo*, Turbomachinery Technical Conference and Exposition.

Rolfes, M., M. Lange, K. Vogeler and R. Mailach (2017). Experimental and Numerical Investigation of a Circumferential Groove Casing Treatment in a Low Speed Axial Research Compressor at Different Tip Clearances. *ASME Turbo Expo*, Turbomachinery Technical Conference and Exposition.

Schnell, R., M. Voges, R. Monig, M. W. Muller and C. Zscherp (2011). Investigation of blade tip interaction with casing treatment in a transonic compressor-part II: Numerical results. *Journal of Turbomachinery* 133 (1),011008-1~011008-11.

Shabbir, A. and J. J. Adamczyk (2005). Flow Mechanism for Stall Margin Improvement due to Circumferential Casing Grooves on Axial Compressors. *Journal of Turbomachinery* 127(4), 708-717.

Suder, K. L., M. D. Hathaway, S. A. Thorp, A. J. Strazisar and MB. Bright (2000.). Compressor Stability Enhancement Using Discrete Tip Injection. *ASME Turbo Expo*, Power for Land, Sea, and Air.

Sun, D., J. Li, X. Dong, B. Gu and X. Sun (2018). Effects of Rotating Inlet Distortion on Two-Stage Compressor Stability with Stall Precursor-Suppressed Casing Treatment. *ASME Turbo Expo*, Turbomachinery Technical

Conference and Exposition.

Sun, X., D. Xu and D. Sun (2019). Recent development of casing treatments for aero-engine compressors. *Chinese Journal of Aeronautics* 32 (1), 1-36.

Taghavi-Zenouz R., Behbahani M. H. A. (2018). Improvement of aerodynamic performance of a low speed axial compressor rotor blade row through air injection. *Aerospace Science and Technology* 72, 409-417.

Voges, M., C. Willert, R. Monig and H. P. Schiffer (2013). The effect of a bend-slot casing treatment on the blade tip flow field of a transonic compressor rotor. *ASME Turbo Expo 2013*, Turbine Technical Conference and Exposition.

Wang, W., J. Lu, X. Luo and W. Chu (2020). Failure mechanism of slot casing treatment in improving stability of a Highly-Loaded Axial Compressor Stage. *Aerospace Science and Technology 105, 105979*.

Wang, W., W. Chu and H. Zhang (2014). The effect of injector size on compressor performance in transonic axial compressor with discrete tip injection. *Proceedings of the Institution of Mechanical Engineers, Part A: Journal of Power and Energy* 228 (7),760-771.

Wang, W., W. Chu and H. Zhang (2015). Numerical investigation on the effect of a plenum chamber with slot-type casing treatment on the performance of an axial transonic compressor. *Proceedings of the Institution of Mechanical Engineers, Part A: Journal of Power and Energy* 229 (4),393–405.

Wang, W., W. Chu and H. Zhang (2018). Mechanism study of performance enhancement in a subsonic axial flow compressor with recirculating casing treatment. *Proceedings of the Institution of Mechanical Engineers, Part G: Journal of Aerospace Engineering* 232(4),680-693.

Wang, W., W. Chu, H. Zhang and H. Kuang (2017). Experimental and numerical study of tip injection in a subsonic axial flow compressor. *Chinese Journal of Aeronautics* 30 (3),907-917.

Wang, W., J. Lu, X. Luo and W. Chu (2019). Coupling Method of Stability Enhancement Based on Casing Treatments in an Axial Compressor. *Aerospace Science and Technology* 95 (105449),1-13.

Wilke, I., H. P. Kau and G. Brignole (2005). Numerically Aided Design of a High-efficient Casing Treatment for a Transonic Compressor. *ASME Turbo Expo 2005*, Gas Turbie Technology.

Yang, L., Q. Zheng, A. Lin and M. Luo (2020). Unsteady performance and thermodynamic analysis of aero-engine compressor at different water ingestion conditions. *International Journal of Energy Research* 44(8), 6567-6582.

Zhang, H., Y. Wu, Y. Li, X. Yu and B. Liu (2019). Control of compressor tip leakage flow using plasma actuation. *Aerospace Science and Technology* 86,244-255.